Humidity, Temperature and Pressure Effects in an Electrostatically Enhanced Heat Exchanger

M.M. Ohadi[1], S.S. Li[2], J.M. Webber[3], S.W. Kim[4] and R.L. Whipple[4]

Humidity, temperature, and pressure effects on corona discharge, heat transfer enhancements and pressure drop characteristics were studied in a gas-to-gas heat exchanger with air as the working fluid in both the tube and shell sides. The humidity and temperature experiments were performed at several electrode potentials and for Reynolds numbers that covered a fully laminar to a fully turbulent flow regime. Experiments on effect of pressure included the "I-V" measurements and characteristics of the corona discharge for negative and positive field polarities at various pressures. It is demonstrated that the humidity, temperature and pressure have well defined effects on corona discharge currents. However, their effects on heat transfer enhancements and pressure drop characteristics are not as clearly defined, due to the complex mechanism by which interaction of the corona-induced secondary motions and the main flow takes place.

INTRODUCTION

Convective heat transfer enhancement via corona discharge utilizes the effect of electrically-induced secondary motions to destabilize the thermal boundary layer near the heat transfer surface, leading to substantially higher heat transfer coefficients at the wall. Study of the technique for basic pipe flow and flat plate configurations has been the subject of many experimental and theoretical efforts in the past. Examples include the work by Velkoff [1], Schnurr [2], Mizushina et al. [3], and Kulacki et al. [4]. A survey of the literature up to the mid-1970's is provided by Jones [5]. The subject has recently reached the standard texts, where Davidson and Kulacki [6] provide the fundamental equations governing electrohydrodynamic (EHD) enhancement of convective heat/mass transfer. Review of the more recent work with applications in heat exchangers is given by Ohadi et al. [7,8].

Basic study of EHD heat transfer enhancements in pipe flows and in gas-to-gas heat exchangers has been the subject of an experimental investigation by our EHD group in the past few years. Heat transfer enhancements and pressure drop characteristics as a function of flow, and electric field parameters of basic pipe flows, were reported in Ohadi et al. [9] and Nelson et al. [10]. Results corresponding to EHD enhancement of heat transfer and its effect on pumping power requirements in a shell-and-tube heat exchanger were reported in [7]. Experiments included individual and simultaneous excitation of the tube and shell sides as a function of flow and electric field parameters.

The present paper is concerned with continuation of the work reported in [7] and the

1. Present address : Department of Mechanical Engineering, Sharif University of Technology, Tehran, I.R. Iran
2. Department of Mechanical Engineering, University of Maryland, College Park, MD 20742.
3. Present address : Car Product Development Division, Ford Motor Co., Dearborn, MI 48121-2053.
4. Department of Mechanical Engineering/Engineering Mechanics, Michigan Technological University, Houghton, MI 49931, USA.

Scientia Iranica, Vol. 1., No. 1, © Sharif University of Technology, April 1994.

preliminary findings presented in [8]. Specifically, the effect of humidity, temperature, and pressure on EHD heat transfer enhancements and corona discharge characteristics for air flow in a tube, augmented with a co-axial wire electrode, were studied. The humidity and temperature experiments were performed in a gas-to-gas heat exchanger. The pressure effect experiments employed a separate experimental apparatus, as will be described in the next section.

A thorough search of the literature, as documented in Webber [11], failed to identify any previous study that has addressed the conditions investigated here. Limited experimental results on effect of humidity on corona discharge in sphere gaps, varying between 20 to 250 mm in diameter, are given in Kuffel and Zaengl [12]. It is shown that the breakdown voltage increases with the partial pressure of water vapor. A study by White [13] investigated the influence of temperature, pressure, and humidity on "I-V" characteristics for negative corona discharge in air. The experiments were performed in a pressure vessel under no-flow conditions and at pressures much higher than those reported here. Miller and Leob [14] investigated the effect of pressure on current-voltage characteristics for two concentric cylinders. The experiments were performed for very low currents (10^{-6} to 10^{-12}A) and at very high voltages (in the vicinity of 100 kV). None of the previous studies has dealt with the fluid property effects on electrostatic heat transfer enhancement in a forced convective flow.

EXPERIMENTAL APPARATUS AND PROCEDURE

Humidity and Temperature Effect Experiments

Essential features of the experimental apparatus for humidity and temperature effect experiments are shown in Figure 1. As seen there, the tube-side of a shell-and-tube heat exchanger served as the test section in the present experiments. The overall apparatus consisted of four main segments: (1) the heat exchanger, (2) the high-voltage circuitry and electrode tensioning mechanism, (3) the heating energy supply circuitry, and (4) the air handling system. A brief description of these components will be given in the following, with complete details available in Webber [11].

The Heat Exchanger

The experiments were performed on the tube-side of the shell and-tube heat exchanger shown in Figure 1. The shell-side of the heat exchanger operated at a fixed Reynolds number and at zero-electric field potential in all experiments. The shell side simply acted as a heat sink, facilitating heat rejection from the tube-side. The heat exchanger consisted of two concentric tubes, both made of aluminum (6061-T6) tubing. Two plexiglas disks, each 25.4 mm (1.0 in) thick, served as the end caps for the heat exchanger. They provided visual observation of the corona while serving as electrical insulators at the heat exchanger ends. Measurement of temperatures at the heat exchanger inlet and exit ports was performed via type E gauge 30 thermocouples. All thermocouple voltages were read and recorded by a $5\frac{1}{2}$ digit computer-interfaced multimeter.

The Electrode Circuitry

Application of the high-voltage electric field to the tube-side was through a 0.25 mm (0.010 in) stainless steel (AISI 304) wire which was coaxial with the tube axis, as shown in Figure 1. Supply of electric field to the electrode was via a high-voltage (0-30 kV), low-current (10-15 mA) DC power supply. To minimize any end effects, the tube-side electrode ran the length of the heat exchanger and extended 15 cm (equivalent to ≈ 5 test section tube inner diameters) into the inlet and exit sections. At the upstream end, the electrode was joined to a length of braided dacron fishing line which was connected to a

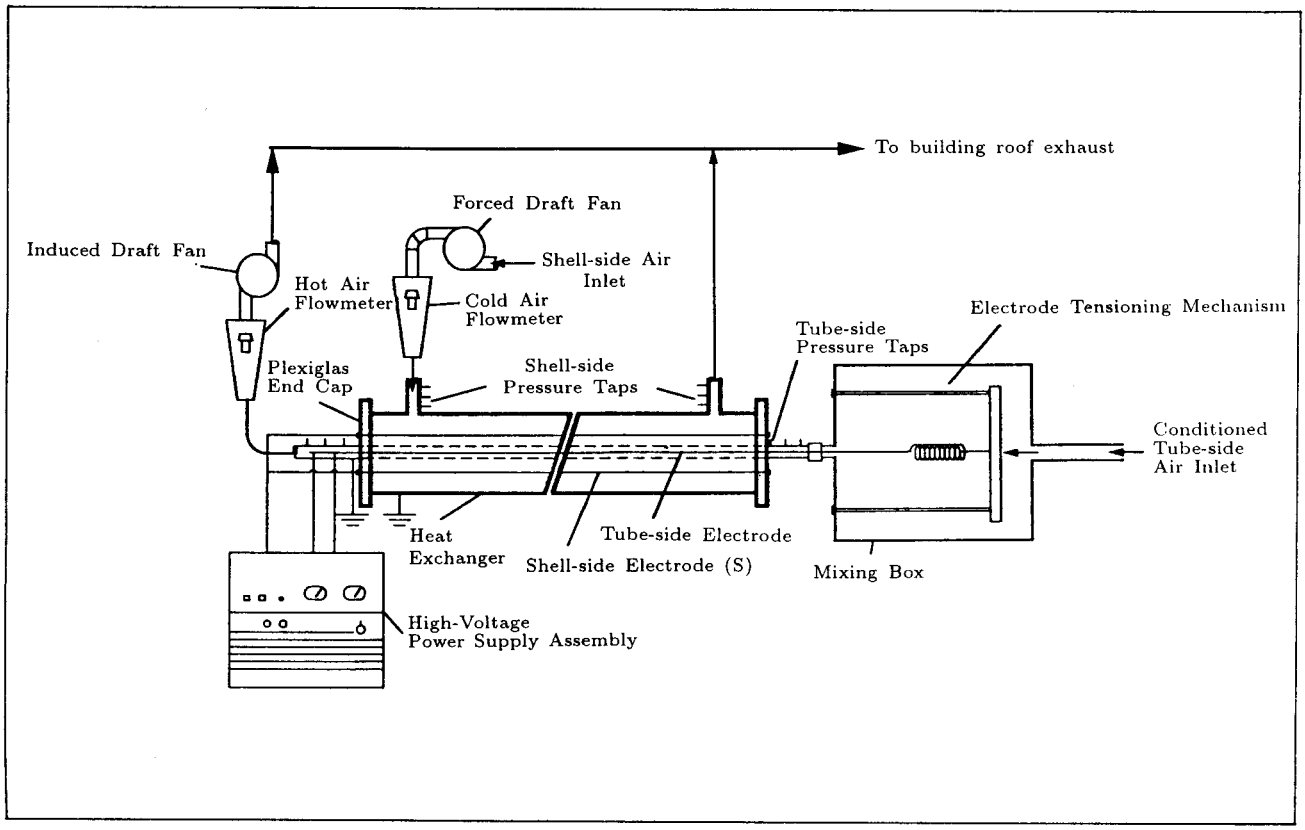

Figure 1a. Schematic of the heat exchanger test apparatus.

spring-loaded electrode tensioning mechanism. To eliminate residual kinks and non-uniformities, the electrode was "aged" under tension for 24 hours prior to installation.

Other Apparatus Components

Humidity control for flow entering the heat exchanger was through use of a humidifier and a desiccant bed dryer (Figure 1b). By adjusting the flow rate of air leaving the dryer and the water vapor exiting the humidifier, a desired humidity level was achieved. Air was used as the working fluid in both the tube and shell sides. Heating of air for the hot side of the heat exchanger (here, the tube-side) was provided through a series of resistive heating elements which were attached to a ceramic base plate and housed in the flow delivery tube upstream of the heat exchanger as shown in Figure 1b. Care was taken to ensure that uniform heating of air in the tube was powered with a regulated low-voltage DC power supply. Mixing of the air before it entered the heat exchanger was accomplished with a mixing box upstream of the heat exchanger. The mixing box also housed the electrode tensioning mechanism for the tube-side (Figure 1a). An induced-draft fan supplied the air flow through the tube-side and into a flow meter and a control valve before it was exhausted to the building roof. Air flow to the shell side of the heat exchanger was supplied via a forced-draft fan on the upstream end of the heat exchanger. Use of separate flow meters and control valves for the hot and cold sides allowed independent control of flow rate through the tube and shell sides. Measurement of volumetric flow rates in the tube and shell sides was via rotameters which were calibrated to 0.5% of their full scale.

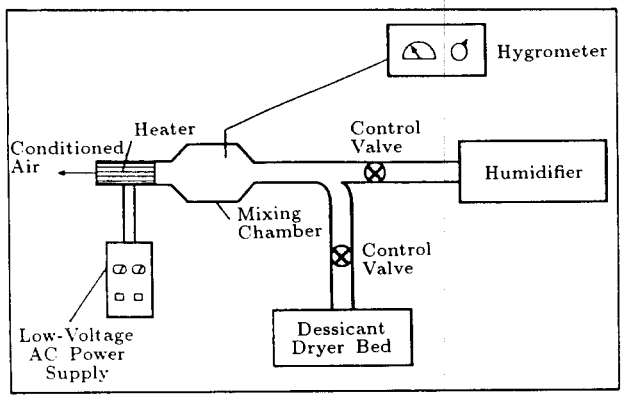

Figure 1b. Schematic of the humidity control apparatus.

Pressure Effect Experiments

The experimental set up for the effect of pressure experiments is schematically shown in Figure 2. A 0.13 mm diameter stainless steel wire located along the center line of a 25.4 cm-long stainless steel tube with 3.81 cm ID and 4.76 cm OD, served as the electrode. The test section tube had two plexiglas windows glued at its ends which provided visual observation of the corona discharge. Room air was introduced into the tube through a moisture trap, a flow meter, and a mercury manometer and exhausted by a rotary vacuum pump.

A DC power source (80 kV and 5 mA) with a variable transformer was connected to the electrode via a 150 W light bulb to limit the excess current flow. The lamp in effect protected the loop from an accidental current surge. Current and voltage were measured with a digital multimeter and a high-voltage probe with a digital oscilloscope or a kilovolt meter, respectively. Experiments were performed as a function of pressure (which ranged from nearly zero to 740 torr), and applied corona voltage (which ranged from 2 to 15 kV). Further details

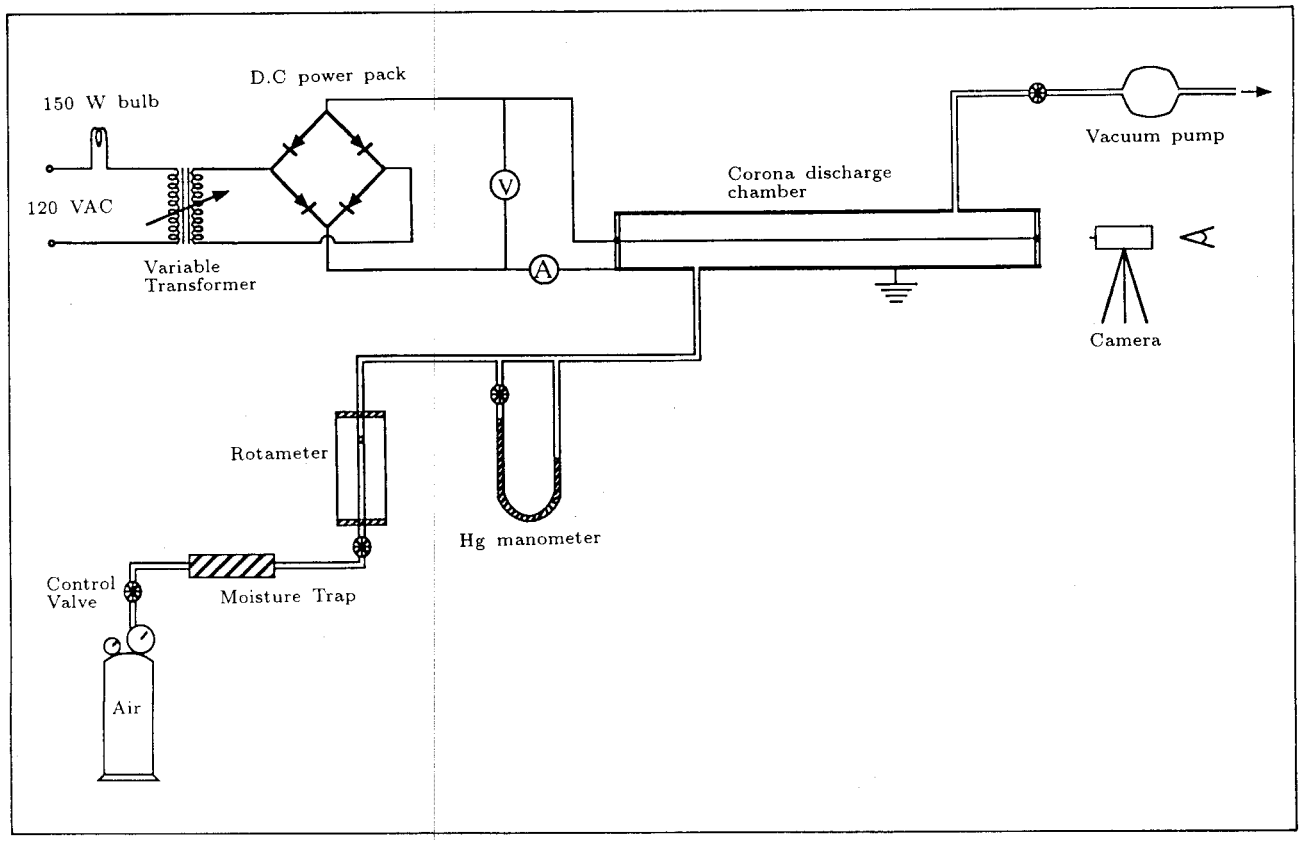

Figure 2. The apparatus for pressure effect experiments.

of the pressure effect apparatus can be found in [11].

DATA REDUCTION

The overall heat transfer coefficient U for the heat exchanger was determined from the defining equation.

$$U = \frac{\dot{Q}}{(A)(LMTD)}, \tag{1}$$

where $\dot{Q}$ is the net rate of heat transfer between the hot and cold fluids, and A is the heat transfer surface area based on the tube-side outer surface area given by

$$A = \pi D_{t,o} l, \tag{2}$$

in which l is the effective heat exchanger length (the length over which heat transfer takes place) and $D_{t,o}$ is the tube-side outer diameter. The log mean temperature difference for the heat exchanger is defined as

$$LMTD = \frac{(T_{bt,i} - T_{bs,e}) - (T_{bt,e} - T_{bs,i})}{ln\left[\frac{(T_{bt,i} - T_{bs,e})}{(T_{bt,e} - T_{bs,i})}\right]}, \tag{3}$$

in which $T_{bt,i}$ and $T_{bt,e}$ represent average tube-side fluid bulk temperatures at the inlet and exit of the heat exchanger. The corresponding temperatures for the shell-side are $T_{bs,i}$ and $T_{bs,e}$, respectively. In each case, the mean fluid bulk temperature was determined by taking the average of measurements at several positions across the tube cross section. This practice was necessary to resolve cross stream temperature variations which could particularly be significant in laminar flow cases.

The rate of heat transfer $\dot{Q}$ was obtained by writing an energy balance equation for the tube-side to yield

$$\dot{Q} = \dot{m}_t C_{p,t}(\bar{T}_{bt,i} - \bar{T}_{bt,e}) + \dot{Q}_c, \tag{4}$$

where $\dot{m}_t$ and $C_{p,t}$ are mass flow rate and specific heat of air in the tube-side. Equation 4 assumes negligible axial heat conduction losses. This was a reasonable assumption since the plexiglas end caps and use of insulating spacers minimized such losses. The quantity $\dot{Q}_c$ is the joule heating associated with corona discharge in the test section estimated as

$$\dot{Q}_c = \left[I\frac{l}{L}\right] E, \tag{5}$$

where I is the total measured current for the entire length L of the electrode, while l represents that portion of electrode that spans the heat exchanger test section length. The quantity E is the measured electric potential difference between the tube-side electrode and the grounded wall.

The Reynolds number used in parameterization of the results for the tube-side was evaluated from

$$Re_t = \frac{4\dot{m}_t}{\mu_t \pi D_{t,i}}. \tag{6}$$

Similarly, the shell side Reynolds number was evaluated from

$$Re_s = \frac{4\dot{m}_s}{\mu_s \pi (D_{s,i} + D_{t,o})}. \tag{7}$$

The quantities $\dot{m}_t$ and $\dot{m}_s$ in Equations 6 and 7 are measured mass flow rates in the tube and shell sides of the heat exchanger, respectively. The viscosities μ_t and μ_s were evaluated for pure air at the tube and shell side average fluid bulk temperatures, respectively. The quantities $D_{t,i}$ and $D_{t,o}$ refer to the inner and outer diameters of the tube-side while $D_{s,i}$ represents inner diameter of the shell side, respectively.

The pressure drop measurements between the inlet and exit of the heat exchanger test

section were nondimensionalized by the velocity head $1/2\rho u^2$ to yield pressure drop coefficient K_p as

$$K_{p,t} = \frac{\Delta P_t}{\frac{1}{2}\rho_t \bar{u}_t^2}, \tag{8}$$

in which ΔP_t, ρ_t, and $\bar{u}_t$ refer to pressure drop, density and average fluid velocity in the tube-side of the heat exchanger, respectively. The average velocity $\bar{u}_t$ in Equation 8 was determined from measurement of the corresponding mass flow rate $\dot{m}_t$. The density ρ_t was evaluated at the mean pressure and temperature in the test section using the ideal gas equation of state. This assumption was found very reasonable for the range of pressures and temperatures in the present experiments. The pressure drop ΔP_t was measured directly by appropriately positioned pressure taps at the inlet and exit of the heat exchanger, as shown in Figure 1a.

RESULTS AND DISCUSSION

The heat transfer enhancement results are expressed in terms of the ratio of overall heat transfer coefficient U in the presence of the applied electric field ($U_{E\neq 0}$) to that of the zero electric field condition ($U_{E=0}$). With the zero-field experiments serving as the base case, the enhancement ratios ($U_{E\neq 0}/U_{E=0}$) should be free of any undetected systematic errors that may have existed in the experimental apparatus or procedure. The overall heat transfer coefficient U was determined from Equation 1, based on temperature measurements at the inlet and exit of the heat exchanger. Due to presence of the high-voltage field in the test section, measurement of local temperatures was not possible. Therefore, no information is available on individual film coefficients in the tube and shell sides, precluding reporting of the results in terms of their corresponding Nusselt numbers. The electric field parameters are expressed in terms of direct dimensional quantities. The reason for choosing to go with this option is described in Ohadi et al. [9].

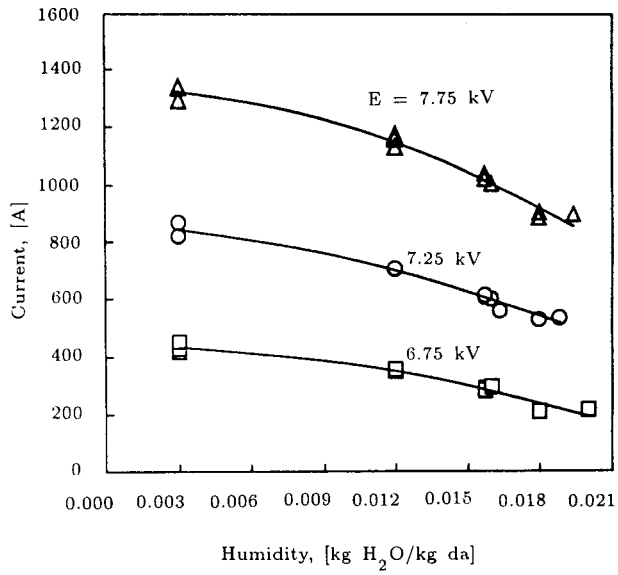

Figure 3. Effect of humidity on discharge current.

Effect of Humidity

Figure 3 presents distribution of the corona discharge current as a function of working fluid humidity at three different electrode potentials. The Reynolds number for the data in Figure 3 ranged from a fully laminar (Re = 1000) to a fully turbulent (Re = 7500) condition. In each case three humidity levels, corresponding to absolute humidity of $\omega = 0.003, 0.012$, and 0.018 kg H_2O/(kg da) were examined. At an average room temperature of 22° C these correspond to relative humidity of $\approx$ 15%, 70%, and oversaturated (Rh > 100%), respectively. The data in Figure 3 suggest that an increase in flow humidity results in a marked decrease in the corona discharge current. This is consistent with the visualization experiments reported in [15] which demonstrated that a strong suppression in streamer propagation in both the axial direction and in branching was observed when air was saturated with water vapor. However, in that study the experiments were performed with a point-to-plate electrode configuration in a chamber under atmospheric pressure. Figures

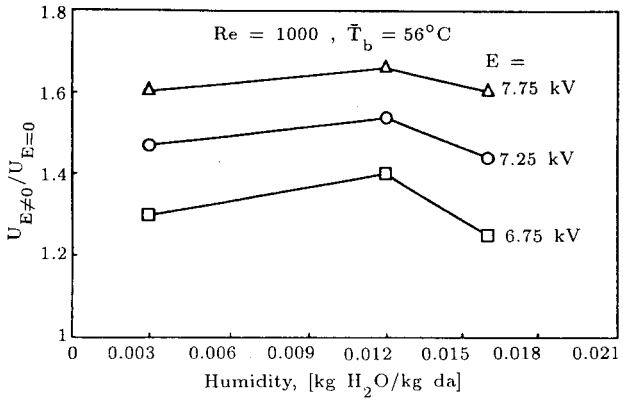

Figure 4a. Effect of humidity on heat transfer enhancement, Re = 1000.

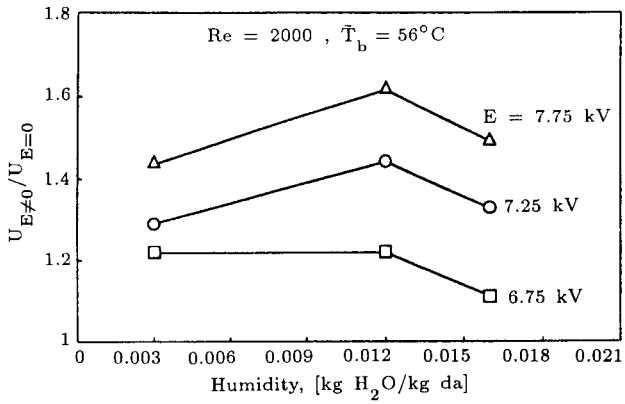

Figure 4b. Effect of humidity on heat transfer enhancement, Re = 2000.

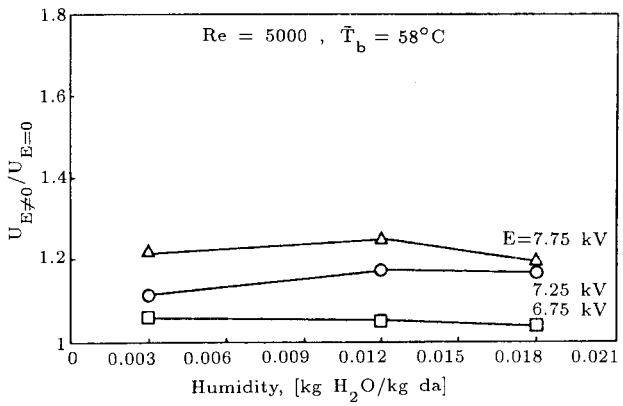

Figure 4c. Effect of humidity on heat transfer enhancement, Re = 5000.

4a through 4c depict heat transfer enhancements as a function of humidity content for Reynolds numbers 1000, 2000, and 5000, respectively. For Re > 5000 no enhancements were obtained as the strong turbulence eddy diffusivity effect overwhelmed the influence of corona-induced secondary motions for the single-electrode configuration in the present experiments. With higher electric current densities (e.g., through use of multi-electrodes) it is possible to extend enhancements into higher Reynolds numbers, as demonstrated in [9].

From the overall inspection of the data in Figures 4a-4c it is seen that maximum enhancements take place at the mid-humidity level ($\omega = 0.012, \mathrm{Rh} = 70\%$) and decrease there after with further increase in the humidity. For the range of parameters in the present experiments, a reduction of 10 to 15% in heat transfer enhancements at the supersaturated condition (Rh > 100%) is observed. The pressure drop data in Figures 5a-5c follow a trend similar to their corresponding heat transfer enhancement curves. The corona-induced streamers give rise to the production of secondary motions that are essential to the EHD heat transfer enhancement mechanism. Therefore, the reduced enhancement at the supersaturated condition in Figures 5a-5c is consistent with the above-mentioned decrease in the streamer propagation experiments reported by Leob [15].

With respect to the accuracy of the data, detailed uncertainty analysis of the overall heat transfer coefficient U indicated uncertainties that ranged from a minimum of 7.8% to a maximum of 16.9% with an average uncertainty of ±11.1% for the range of parameters reported here. The corresponding average uncertainty for the pressure drop coefficient K_p was 9.2%. The compound uncertainty calculations took into account the effects of both bias and precision errors for all quantities involved. Details of the uncertainty calculations and their analysis are given in Webber [11].

Effect of Temperature

Figure 6 presents current versus voltage variations at average fluid bulk temperatures of

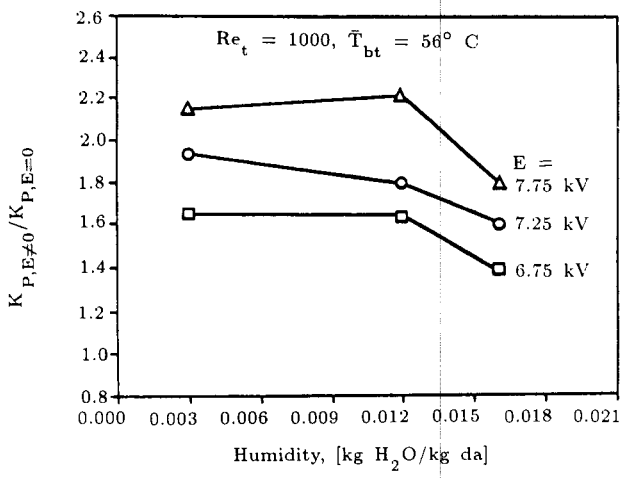

Figure 5a. Effect of flow humidity on pressure drops, Re = 1000.

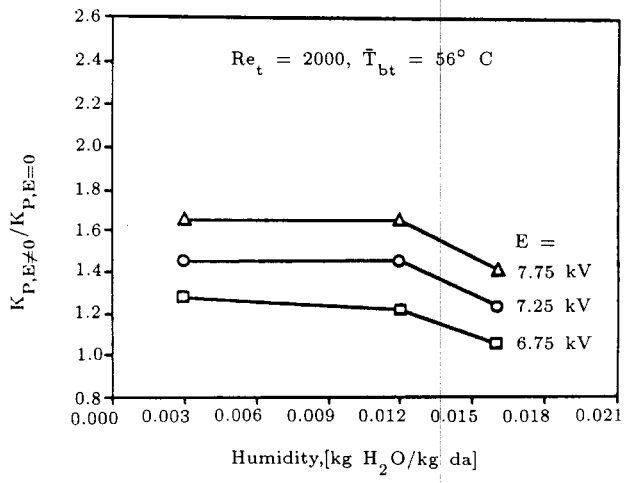

Figure 5b. Effect of flow humidity on pressure drops, Re = 2000.

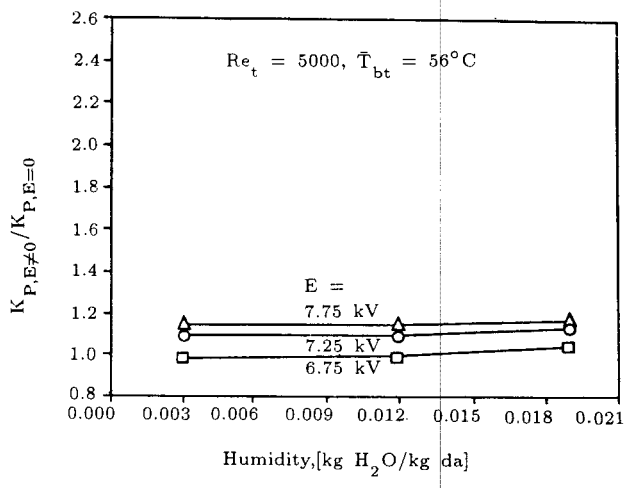

Figure 5c. Effect of flow humidity on pressure drops, Re = 5000.

20, 65, and 80° C. The absolute humidity in this set of experiments was kept at $\omega = 0.012$ (kg H_2O)/(kg dry air). Results are reported for Reynolds numbers of 2000, 5000 and 10,000. From the data in Figure 6, two general observations can be identified. First, the "I-V" data appear to be independent of the Reynolds number for the range of parameters studied. This is consistent with the finding in Nelson et al. [10] which was shown to be due to a much higher drifting of the free charges when compared to that of the bulk flow. Second, higher gas temperatures result in higher corona discharge currents. This latter effect can be attributed to the increase of the ionic mobility with the increase in temperature. The increase in ionic mobility in turn raises the drifting velocity of the free charges, thus the discharge current [12].

Effect of temperature on heat transfer enhancements for Reynolds of 1000, 2000 and 5000 are shown in Figures 7a through 7c. The corresponding pressure drop data are shown in Figures 8a through 8c, respectively. It is seen that at the two lower Reynolds numbers, Re = 1000 and 2000, higher working fluid temperatures result in lower heat transfer enhancements. This is contrary to the expectation of a trend

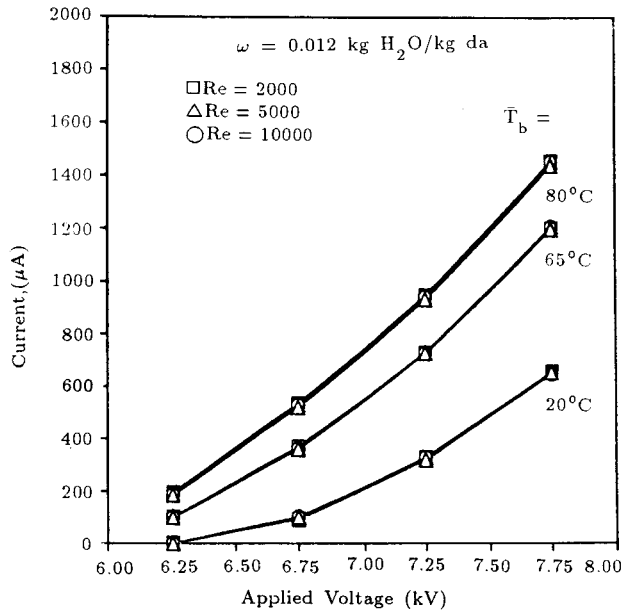

Figure 6. Effect of flow temperature on discharge current.

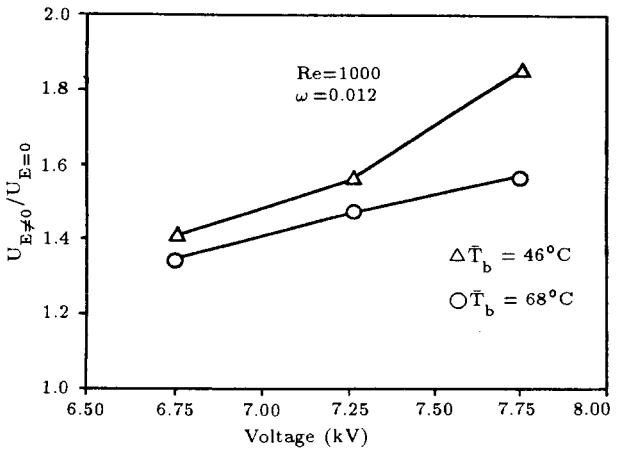

Figure 7a. Effect of temperature on heat transfer enhancements, Re = 1000.

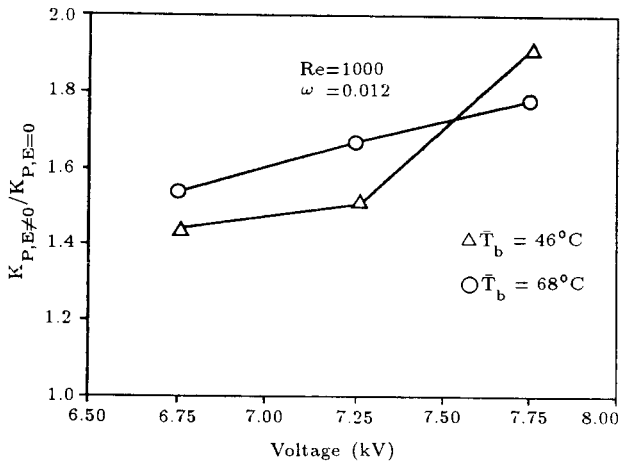

Figure 8a. Effect of temperature on pressure drops, Re = 1000.

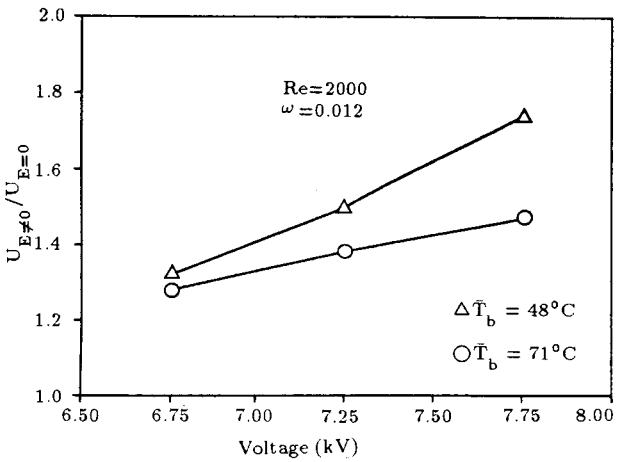

Figure 7b. Effect of temperature on heat transfer enhancements, Re = 2000.

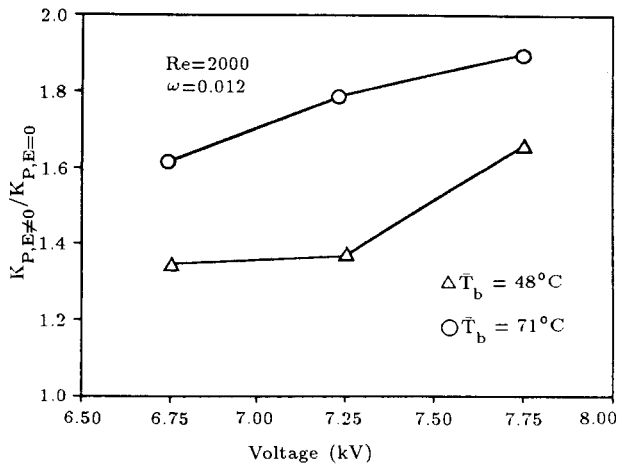

Figure 8b. Effect of temperature on pressure drops, Re = 2000.

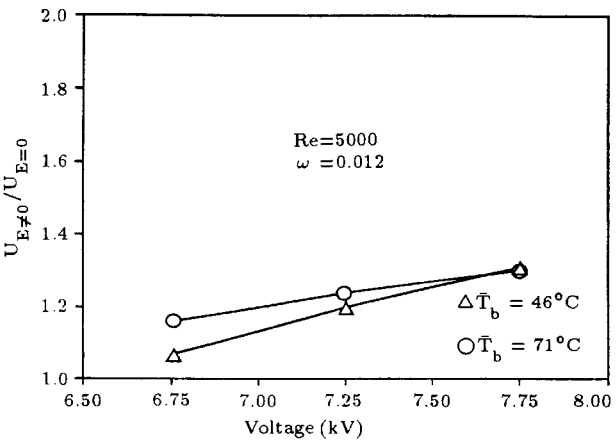

Figure 7c. Effect of temperature on heat transfer enhancements, Re = 5000.

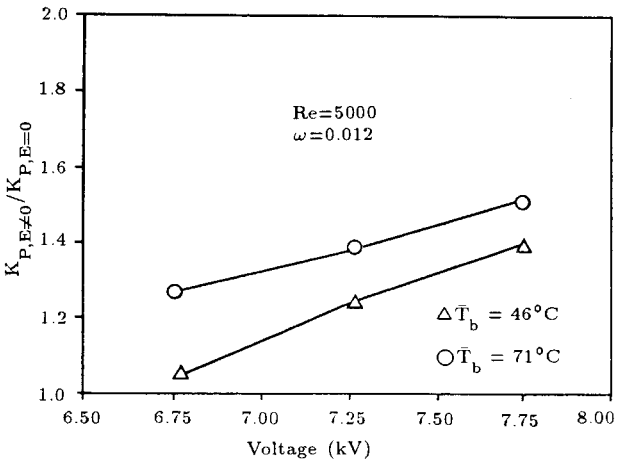

Figure 8c. Effect of temperature on pressure drops, Re = 5000.

similar to that of the higher discharge currents in Figure 6. Calculation of the corresponding Rayleigh number at the average bulk and wall temperatures yielded values number on the order of Ra $\approx 10^8$. At Reynolds of 1000 and 2000 this Rayleigh number suggests a mixed (free plus forced) convection regime, according to the criteria established by Metais and Eckert [16]. The buoyancy-driven secondary motions associated with the mixed convection may have destroyed the well defined EHD-induced secondary motion patterns [9] between the electrode and the heat transfer wall, leading to reduced net EHD enhancements at the wall. As shown in Figure 7c, at Re = 5000, where stronger forced convection effects are present, higher enhancements are initiated at higher temperatures. However, with increase in the field potential, the added corona-induced joule heating effect promotes self-heating of the flow which in turn leads the enhancements in a direction similar to that in Figures 7a and 7b. From a corona discharge viewpoint, the electrically-induced secondary flow is caused by the unbalanced electric body force. This body force is the product of the charge density and the strength of the electric field which reduces to the ratio of the current density over ion mobility. The increase in temperature will cause an increase in both the current density and the ionic mobility such that the net effect will be a reduction in the magnitude of the electric body forces.

Effect of Pressure

Due to experimental limitations, the pressure effect experiments were limited to the study of the pressure effect on corona discharge currents. However, realizing that the electrostatic enhancement mechanism is a current-driven phenomenon, the current magnitudes should generally be an indication of the expected heat transfer enhancements. Both positive and negative electric field polarities were examined in the present experiments. The current-voltage characteristics for positive and negative polarities at various pressures are shown in Figures 9 and 10, respectively. Comparison of current distributions with respect to pressure at a given voltage and at a given current are provided in Figures 11 and 12, respectively. Variations of the threshold voltage with the gas pressure for positive and negative polarities are given in Figure 13.

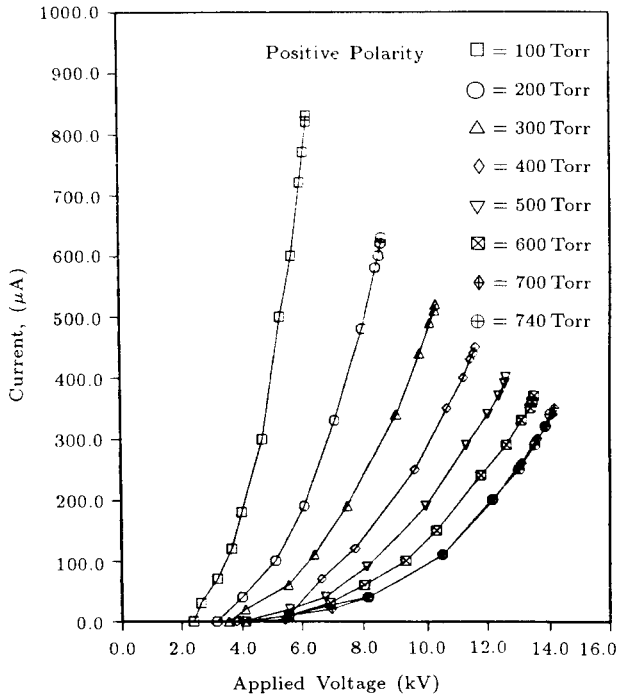

Figure 9. Effect of pressure on "I-V" characteristics, positive polarity.

From the data in Figures 9 and 10, it is seen that for both positive and negative polarities the corona current decreases with increasing pressure. At higher pressures, ionization is greatly reduced by shorter mean free paths of ions, thereby reducing the corona current. At a given current, the voltage increases linearly with increasing the pressure and is consistently higher for positive corona than that of the negative corona (Figure 11). On the other hand, at a given voltage the corona current decreases rapidly with increasing pressure (Figure 12). Moreover, the data in Figure 12 suggest that, at low pressures, the current discharge in the negative corona is much higher than that of the positive corona at a given voltage. This lower

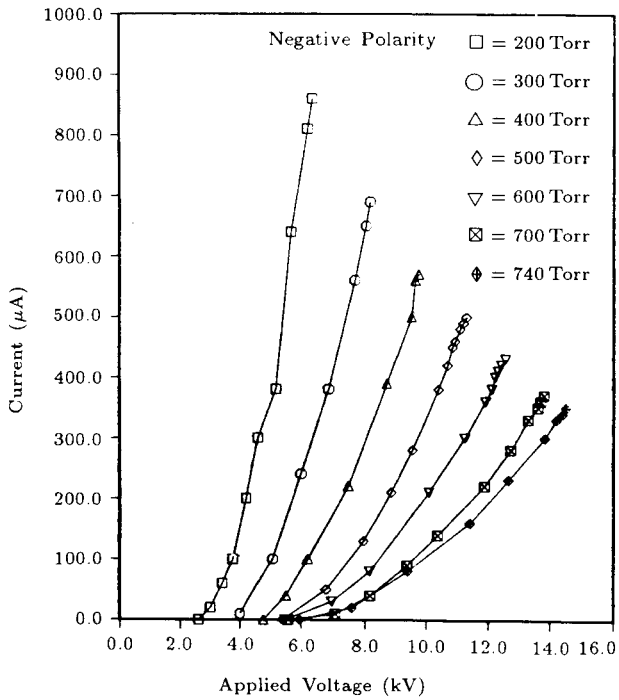

Figure 10. Effect of pressure on "I-V" characteristics, negative polarity.

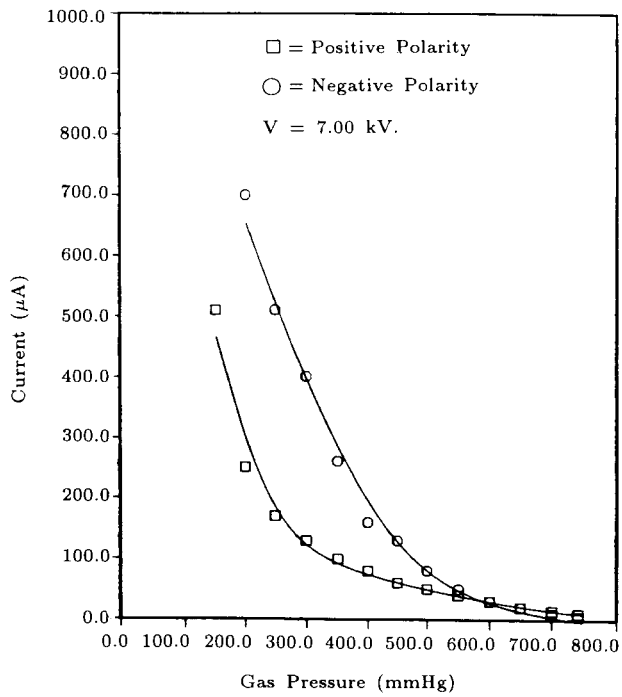

Figure 12. Effect of pressure on positive and negative polarities at a given current.

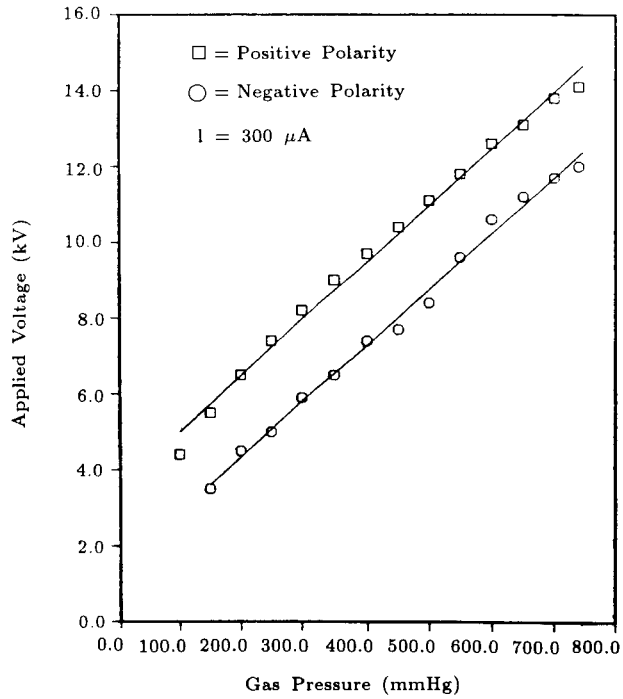

Figure 11. Effect of pressure on positive and negative polarities at a given voltage.

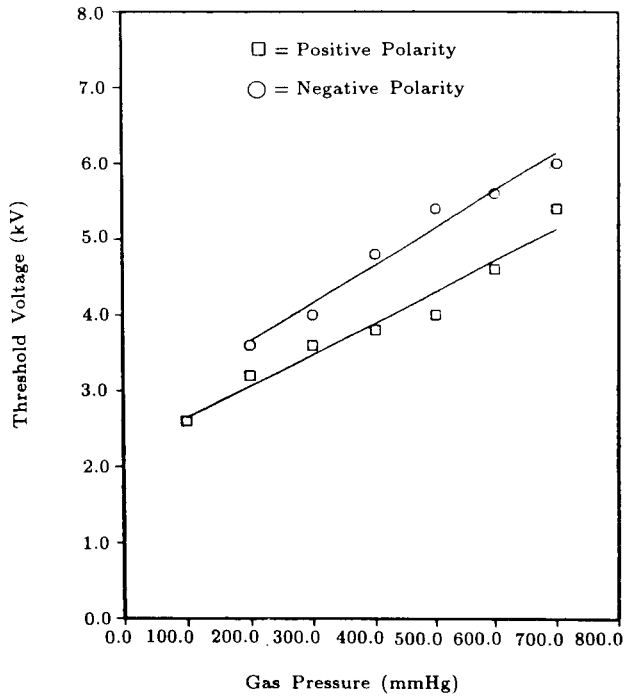

Figure 13. Effect of pressure in threshold voltage or positive and negative polarities.

current can be attributed to the suppressing space charge produced by the large number of ions in a positive corona field. Variations of the threshold voltage with the gas pressure in Figure 13 suggests that the threshold voltage increases with increasing pressure, and it is somewhat higher in a negative corona than in a positive corona.

CONCLUSIONS

Effects of working fluid humidity, temperature, and pressure on corona discharge characteristics and heat transfer enhancements for forced convection flow were studied experimentally in a gas-to-gas, EHD-enhanced heat exchanger. The humidity and temperature experiments were performed at several electrical potentials between the threshold and spark-over limits and for Reynolds numbers that covered a fully laminar to a fully turbulent flow regime. It was found that a higher humidity resulted in a lower corona discharge current. At a given electric potential, maximum enhancements took place at the mid-humidity level ($\omega = 0.012$). With further increase in the humidity, enhancements decreased by 10 to 15% below their maximum value for the range of parameters studied here. At a given humidity content and electric potential, maximum enhancements corresponded to Reynolds numbers in the laminar/transitional zone. Higher working fluid temperatures resulted in higher corona discharge currents. However, the increase in the ionic mobility coupled with the buoyancy-induced secondary motion effect at high temperatures and low Reynolds numbers suppressed the EHD heat transfer enhancement rates.

With respect to the effect of pressure, it was found that an increase in the gas pressure resulted in a rapid decrease in the corona discharge current. The threshold voltage increased with increased pressure for both positive and negative field polarities. Moreover, at a given pressure, its magnitude was higher for the negative corona than it was for the positive corona.

ACKNOWLEDGEMENTS

The support of this work by the Gas Research Institute, under contract No.5087-260-1528, is greatly acknowledged. The assistance of Ms. Y. Flad in preparation and technical proofreading of this manuscript is highly appreciated.

NOMENCLATURE

A	Heat transfer surface area
C_p	Specific heat of air
$D_{s,i}$	Inner diameter of shell
$D_{t,i}$	Inner diameter of tube
$D_{t,o}$	Outer diameter of tube
E	Applied electric potential
I	Total measured corona current
$K_{p,t}$	Tube-side pressure drop coefficient
l	Effective electrode length
L	Total electrode length
$LMTD$	Logarithmic mean temperature difference
$\dot{m}_t$	Tube-side mass flow rate
$\dot{m}_s$	Shell-side mass flow rate
$\dot{Q}$	Heat transfer rate
$\dot{Q}_c$	Corona-induced joule heating rate
Ra	Rayleigh number
Rh	Relative humidity
Re_t	Tube-side Reynolds number
Re_s	Shell-side Reynolds number
$T_{bt,i}$	Average tube-side flow bulk temperature at the heat exchanger inlet
$T_{bt,e}$	Average tube-side flow bulk temperature at the heat exchanger exit
$T_{bs,i}$	Average shell-side flow bulk temperature at the heat exchanger inlet
$T_{bs,e}$	Average shell-side flow bulk temperature at the heat exchanger exit

T_b	Average flow bulk temperature in the test section
$\bar{u}_t$	Mean velocity of tube-side air
$\bar{u}_s$	Mean velocity of shell-side air
U	Overall heat transfer coefficient
$\dot{V}$	Volumetric flow rate
ω	Absolute humidity
μ	Viscosity
ρ	Mass density

Subscripts

b	bulk
i	inlet, inner
o	outer
e	exit, outlet
s	shell
t	tube

REFERENCES

1. Velkoff, H.R. "The effects of ionization on the flow and heat transfer of a dense gas in a transverse electrical field," *Proc., Heat Transfer and Fluid Mech. Inst.*, Univ. of California, Berkeley, CA, Stanford Univ. Press, pp 260-275 (1984).
2. Schnurr, N.M. "The effect of a radial electric field on heat transfer to air flowing through a circular duct," Ph.D. Thesis, Ohio State University (1965).
3. Mizushina, T., Udea, H., Matsumoto, T. and Wage, K. "Effect of electrically induced convection on heat transfer of air flow in an annulus," *J. Chem Engng. Japan,* **9**, pp 97-102 (1976).
4. Kulacki, F.A, Boriah, S. and Martin, S.A. "Corona discharge augmentation of the catalytic combustion of hydrogen in the diffusion controlled regime," *Int. J. Hydrogen Energy,* **6**, pp 73-95 (1981).
5. Jones, T.B. "Electrohydrodynamically enhanced heat transfer in liquids-A review," *Advances in Heat Transfer,* **14**, Academic Press, pp 107-148 (1978).
6. Davidson J.H and Kulacki, F.A. "Convective heat transfer with electric and magnetic fields," in *Handbook of Single-Phase Convective Heat Transfer,* S. Kakca, R. Shah, W. Aung, Eds., John Wiley and Sons, New York (1989).
7. Ohadi, M.M., Sharaf, N. and Nelson, D.A. "Electrohydrodynamic enhancement of heat transfer in a shell-and-tube heat exchanger," *J of Expo Heat Transfer,* **4**, pp 19-39 (1991).
8. Ohadi, M.M., Webber, J.M. and Whipple, R.L. "Effect of working fluid humidity and temperature on EHD heat transfer enhancements in a gas-to-heat exchanger," *Proc, 3rd ASME-JSME Joint Thermal Engineering Conference,* **3**, pp 15-24 (1991).
9. Ohadi, M.M., Nelson, D.A. and Zia, S. "Augmentation of laminar and turbulent forced convection heat transfer in tubes via corona discharge," *Int. J. of Heat and Mass Transfer,* **34** (4-5), pp 1175-1187 (1991).
10. Nelson, D.A. Ohadi, M.M., Zia, S. and Whipple, R.L. "Effect of corona discharge on pressure drop characteristics for forced convection in tubes," *Int. J. of Heat and Fluid Flow,* **11** (4) pp 298-302 (1990).
11. Webber, J.M. "Effect of working fluid properties and impulse corona discharge on electrohydrodynamic heat transfer enhancements in a gas-to-gas heat exchanger, Ph.D. Thesis, Michigan Technological University, Houghton, MI (1990).
12. Kuffel, E. and Zaengl, W.S. *High Voltage Engineering Fundamentals,* Pergamon Press, New York, pp 297-355 (1984).
13. White, H.J. *Industrial Electrostatic Precipitation,* Addison Wesley, MA, pp 74-125 (1963).

14. Miller, C.G. and Leob, L.B. *J. Appl. Phys.*, **22**, pp 494-502, and pp 614-621 (1951).

15. Leob, L.B. *Electrical Coronas, Their Basic Physical Mechanisms,* University of California Press, Berkeley, CA, pp 225-227 (1965).

16. Metais, B. and Eckert, E.R.G. "Forced, mixed, and free convection regimes," *J. Heat Transfer,* pp 295-296 (1964).